Appl. Phys. B (2016) 122:8
DOI 10.1007/s00340-015-6292-9

Applied Physics B
Lasers and Optics

Estimates for production of radioisotopes of medical interest at Extreme Light Infrastructure – Nuclear Physics facility

Wen Luo[1,2] · Mariana Bobeica[1] · Ioana Gheorghe[1,3] · Dan M. Filipescu[1] · Dana Niculae[4] · Dimiter L. Balabanski[1]

Received: 1 September 2015 / Accepted: 17 November 2015

Abstract We report Monte Carlo simulations of the production of radioisotopes of medical interest through photoneutron reactions using the high-brilliance γ-beam of the Extreme Light Infrastructure – Nuclear Physics (ELI–NP) facility. The specific activity for three benchmark radioisotopes, ^{99}Mo/^{99m}Tc,^{225}Ra/^{225}Ac and ^{186}Re, was obtained as a function of target geometry, irradiation time and γ-beam energy. Optimized conditions for the generation of these radioisotopes of medical interest with the ELI–NP γ-beams were discussed. We estimated that a saturation specific activity of the order of 1–2 mCi/g can be achieved for thin targets with about one gram of mass considering a γ-beam flux of 10^{11} photons/s. Based on these results, we suggest that the ELI–NP facility can provide a unique possibility for the production of radioisotopes in sufficient quantities for nuclear medicine research.

Mariana Bobeica: Contributing first author.

✉ Wen Luo
wenluo-ok@163.com

✉ Mariana Bobeica
mariana.bobeica@eli-np.ro

[1] Extreme Light Infrastructure – Nuclear Physics, "Horia Hulubei" National Institute for Physics and Nuclear Engineering, 30 Reactorului, 077125 Bucharest-Magurele, Romania

[2] School of Nuclear Science and Technology, University of South China, Hengyang 421001, China

[3] Faculty of Physics, University of Bucharest, 077125 Bucharest, Romania

[4] "Horia Hulubei" National Institute for Physics and Nuclear Engineering, 30 Reactorului, 077125 Bucharest-Magurele, Romania

1 Introduction

In nuclear medicine, radioisotopes are used for diagnostic and therapeutic purposes. In many medical procedures, radionuclides are combined with other chemical compounds or pharmaceuticals to form a radiopharmaceutical which when administered to the patient can preferentially localize to specific organs or cellular receptors. This property of radiopharmaceuticals allows nuclear medicine ability to image the extent of a disease process in the body. Treatment of a disease based on metabolism, uptake or binding of a ligand, may also be accomplished; in this case, the radiopharmaceuticals rely on the tissue-destructive power of short-range ionizing radiation.

Over 10,000 hospitals worldwide use radioisotopes in medicine, and about 90 % of the procedures are for diagnosis. The use of diagnostic radiopharmaceuticals is growing at over 10 % per year [1]. The advance in the field is based on new achievements of higher sensitivity of the detection systems [2, 3]. Thus, the main advantage of nuclear medicine is the use of tracers at very low concentrations. However, the advantages of nuclear medicine diagnostics require that the radiotracers have relatively high specific activity, such that the injected radiotracer is not accompanied by too many stable isotopes of the same (or a chemically similar) element.

Currently thermal neutron-induced fission and charged-particle reactions with protons are the main production routes for medical radioisotopes [4]. The increasing demand for medical radioisotopes requires more production facilities, along with the investigation of new ways of production and the application of new radioisotopes in both diagnosis and therapy.

Published online: 20 January 2016

Photonuclear reactions can provide an opportunity for the production of neutron-deficient isotopes, but conventional γ-ray sources do not have a flux density sufficiently high to produce radioisotopes with high enough specific activities. Recent advances in laser technology have led to the development of high-peak power lasers in many laboratories worldwide. When focused to an area of a few tens of square microns, the laser radiation can reach intensities of more than 10^{20} W/cm^2 [5] and laser-driven nuclear phenomena can occur. This opens up the opportunity for scientists to study various nuclear phenomena, including the generation of positron, neutron, proton and heavy ion beams [6]. Combing the advanced laser technology with radio-frequency electron accelerator, Compton backscattering (CBS) of a laser pulse from a relativistic electron beam (*e*-beam) has been proved to be an effective approach to producing energy-tunable, intense and quasi-monochromatic X-rays [7–12] or γ-rays [13–16]. Many CBS-based γ-ray facilities have also been recently developed and used for basic research and various applications [16–18]. Further, benefiting from the progress in generation of the laser-plasma-driven electron bunches, many efforts have been done to develop novel all-optical and compact electron-γ sources [19–22]. Since these sources have a relevant component around the giant dipole resonance for photonuclear absorption, it is very useful for photonuclear studies and medical uses [20–23].

Using these new beam facilities, compact targets could be exposed to the gamma radiation and undergo photonuclear reactions such as (γ, n) and (γ, p) to produce new radioisotopes [4]. Such beams can be used as well as to pump a good fraction of the nuclear ground state population via excited levels into an isomeric state. Thus, after a suitable irradiation time, a radioisotope with high specific activity can be produced. Photonuclear reactions with γ-beams of high intensity and large brilliance allow the production of radioisotopes for medical applications, such as ^{47}Sc,^{44} Ti,^{67} Cu,^{103} Pd,^{117m} Sn,^{169} Er,^{195m} Pt or ^{225}Ac, with a higher specific activity than by classical methods [4, 24]. This production method should also enable further clinical applications of the above-mentioned radioisotopes. For example, ^{195m}Pt can be used for therapeutic monitoring of chemotherapy with compounds containing platinum. In this context the Extreme Light Infrastructure – Nuclear Physics (ELI–NP) facility will have a brilliant γ-beam of 10^4 photons/s/eV, ≤0.5 % bandwidth, with $E_\gamma < 19.5$ MeV, which is obtained by CBS of a laser light off an intense *e*-beam ($E_e > 700$ MeV) produced by a warm linac [25]. This will likely provide an opportunity for the production of radioisotopes for medical research. Simulations that model the intense CBS γ-beam interaction with a solid target are necessary to estimate the radioisotope production parameters. In this paper, we present the results of such simulations for three selected cases ^{99}Mo/^{99m}Tc,^{225} Ra/^{225}Ac and ^{186}Re. We have chosen the above cases for the following reasons: (1) ^{99}Mo was chosen because of its well-known (γ, n) cross section [26]; (2) ^{186}Re isotope was chosen because it has the largest (γ, n) cross section of all radioisotopes of interest [26]; (3) ^{225}Ac was chosen to study the possible isotope production with an actinide target.

We simulated the CBS process to produce the γ-beam with the most appropriate parameters, its transport and delivery to the isotopic target for irradiation, and the subsequent isotope production. In these simulations, we have optimized the isotopic target dimensions and the beam parameters, at defined irradiation time intervals such to maximize the isotope production. Using measured and estimated photonuclear cross sections, we obtained, as realistic as possible, the specific activities achievable at ELI–NP, for the above-mentioned radioisotopes. We have shown that the ELI–NP facility will be suitable for production of radioisotopes for medical research and for evaluation of new methods for radioisotope production. This may open new perspectives toward possible radioisotopes production at future γ-beam facilities. In this study, a γ-beam flux of 10^{11} s^{-1} was used in the simulations, which is a conservative estimate for ELI–NP, but such γ-beam fluxes will be achieved in the first phase of operation of the facility. During the facility development, if the γ-beam flux will increase, then the calculated specific activities of the radioisotopes can be easily scaled, accordingly.

2 Methods and materials

2.1 ELI–NP γ-beam simulation

As discussed above, a very brilliant, intense γ-beam, which is produced by incoherent Compton backscattering of direct laser light with a very brilliant and intense *e*-beam, will become available at the upcoming ELI–NP facility [25]. Such facility will deliver a very intense (up to 10^{12} photons/s), brilliant γ-ray beam, ≤0.5 % bandwidth, with energy up to 19.5 MeV. A Yb:Yag laser will be used to produce such a γ-ray beam and its main performances are the following: pulse energy 2 × 0.2 J, wavelength 515 nm, FWHM pulse length 3.5 ps, repetition rate 100 Hz, focal spot size >28 μm and pulse energy stability 1 %. Accordingly, in our simulations we have used a circularly polarized laser with a wavelength bandwidth of 0.05 %, scattering on a relativistic *e*-beam with an energy spread of 0.04 % at a laser incident angle of $\theta_L = 172.5°$.

Using the Monte Carlo method, we have developed a realistic model of laser photon–relativistic electron interaction which takes into consideration the phase space

distribution of the electron and laser beams. In the model, we implemented a physically constrained *e*-beam emittance and spatial distribution and we also considered a Gaussian laser beam. Since the description of the γ-ray production model and its code, as well as its benchmarking process, goes beyond the contexts of this work, more details will be published elsewhere [27].

We combined the γ-beam simulation code with the Geant4 toolkit [28] to model the MeV-class γ-ray production and to study the spectral and flux density distributions of the γ-beam during its transport from the laser-electron interaction point (IP) to the target, through the ELI–NP γ-ray beamline. A realistic model of the γ-ray beam collimation system, which will be installed at ELI–NP, and also the geometry of thin isotopic target of flexible radius placed toward the beam for the production of the radioisotopes of interest, were implemented in the combined code. Using the simulation code, we obtained the γ-beam characteristics at the surface of the irradiated target, which are required for the calculation of the specific activity of radioactive isotopes.

The collimator opening at a small aperture and the irradiation target were located approximately 9.0 and 9.6 m downstream of the IP, respectively. The collimator's role is to stop the low-energy scattered γ-rays that cannot trigger a photonuclear reaction. If the aperture of the collimator is small enough, a well-collimated γ-beam whose scattering angle is smaller than the collimation angle will pass through the collimator and then will arrive at the surface of the irradiation target. Hence, one could optimize the aperture of the collimator to obtain an appropriate bandwidth of the γ-beam in order to cover the most significant part of the reaction cross sections. For example, when the aperture of the collimator was set to 2.5 mm, a collimation angle of ∼0.28 mrad was obtained. Then only almost 15 % of the total CBS γ-rays passed through the collimator and irradiated further the isotopic target. Considering that the total flux of the γ-rays produced at the IP is 1.0×10^{11} γ/s, the flux of the γ-rays that passed through the collimator was of the order of 10^{10} γ/s.

The ELI–NP γ-beam, that will be used to irradiate the target, will be diagnosed by monitoring its energy, flux density and transverse profile. Figure 1 shows the expected CBS γ-beam spectrum and profile at the surface of an isotopic target for a 640 MeV *e*-beam. The end-point (i.e., on-axis) energy of the scattered γ-rays is defined as

$$E_\gamma \approx 2\gamma^2 E_L(1 - \beta \cos\theta_L), \quad (1)$$

where γ is the Lorentz factor of the relativistic electrons, E_L is the photon energy of the incident laser, and θ_L is the laser incident angle with respect to the electron trajectories. For the 640 MeV *e*-beam, the end-point energy of the scattered γ-rays is about 14.7 MeV (Fig. 1), which is slightly higher than the energy at maximum of the ^{100}Mo(γ, n) cross section, ∼14.5 MeV [26, 29]. The average energy of the γ-rays passing through the collimator aperture was 13.9 MeV, and its beam radius at the surface of the target was about 2.5 mm.

For a CBS γ-ray beam, its energy has a strong dependence on the scattering angle. From the far field observation plane, the γ-beam radius can be approximated by the scattering angle since the γ-beam spot size at the IP is extremely small, on the order of tens μm. The γ-rays energy was therefore correlated with the beam radius at the surface of the target isotope (Fig. 2), which was also equal to the target radius. We found that the center of the γ-beam profile had the highest flux density, which corresponds to the end-point energy of the scattered γ-rays. Figure 2 also shows that in the 14.7 and 16.1 MeV γ-beam cases, the energy-radius distribution and the horizontal line at $E_\gamma = 14.5$ MeV, corresponding the energy for the peak of the ^{100}Mo(γ, n) reaction cross section, intersected at two different points (P1 and P2) of the beam radius. The values for the beam radius at P1 and P2 were approximately 0.9

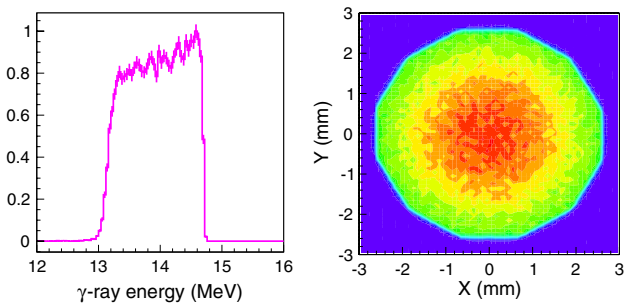

Fig. 1 The γ-beam spectrum (*left*) and transverse profile (*right*) at the surface of the irradiation target. The input *e*-beam energy is $E_e = 640$ MeV, and the collimator opening is 2.5 mm (collimation angle 0.28 mrad)

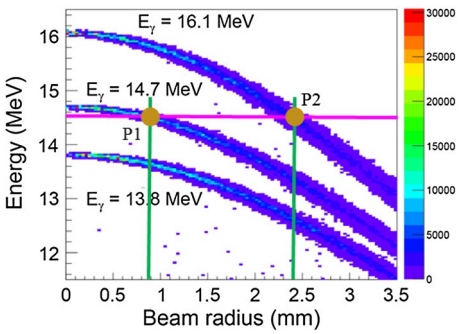

Fig. 2 The correlation between the ELI–NP γ-ray energy and beam radius (the center of the beam corresponds to the zero point on the *x* axis) at the surface of the isotopic target. The *horizontal solid line* represents a photon energy of 14.5 MeV, pointing to the maximum cross section of the ^{100}Mo(γ, n) reaction, ∼150 mb [29]

and 2.5 mm, respectively. The intersection points discussed here indicate a good convolution between the γ-beam spectrum and the reaction cross section, which is crucial for our simulations in order to obtain the highest specific activity, as discussed in the Sect. 3.

2.2 Reactions cross section calculations by EMPIRE

Cross sections of the photon-induced reactions on ^{100}Mo,^{226}Ra and ^{187}Re have been calculated with the modular system EMPIRE 3.2 Malta [29]. Pre-equilibrium emission was taken into account by module PCROSS featuring one-component exciton model with gamma, nucleon and cluster emissions. The compound nucleus mechanism was described by Hauser–Feshbach statistical model. The Koning–Delaroche regional potential for neutrons and protons [30] in the exit channel, the default EMPIRE option for non-actinides, was used. The nuclear level densities were calculated with the Enhanced Generalized Superfluid Model [29]. The Modified Lorentzian 1 closed formula [30] was used for the gamma strength function calculation. The Giant Dipole Resonance (GDR) parameters were retrieved from the RIPL database [30], where parameters deduced from experimental data were available for ^{100}Mo, while parameterizations were used for ^{226}Ra and ^{187}Re. Additional required input parameters were retrieved from the RIPL-3 database [30]. Detailed comparisons between the photonuclear reactions cross sections for ^{100}Mo,^{226}Ra and ^{187}Re from the EMPIRE calculations and those retrieved from the EXFOR database [26] and the TENDL evaluations [31] are given in the Secti. 3. Based on these comparisons, reliably estimated photonuclear reaction cross sections were used in the prediction accurately of the specific activities of the radioisotopes of medical interest.

2.3 Specific activity of radioisotopes and its simulation algorithm

In a typical photonuclear reaction process, the reaction rate P_0 of the target isotope depends upon a number of parameters, such as the number density ρ of target nuclei that are irradiated, the threshold energy of the nuclear reaction E_{th}, the end-point energy of photons E_{max}, the probability of a photonuclear reaction defined by the reaction cross section $\sigma(E_\gamma)$ and the photon flux density. While taking into account the attenuation coefficient of γ-photons inside the target, the reaction rate can be written as:

$$P_0 = \int_{E_{\mathrm{th}}}^{E_{\mathrm{max}}} \int_0^R \frac{\rho N_A}{\mu M} \sigma(E_\gamma) I(E_\gamma, r)[1 - \exp(-\mu L)] \mathrm{d}E_\gamma \mathrm{d}r, \quad (2)$$

where M is the molar mass (g/mol) of the target isotope, $I(E_\gamma, r)$ is the γ-ray linear flux density at the surface of the isotopic target after the polar-angle integration, μ is the linear attenuation coefficient, R is the target radius, L is the target thickness with respect to the direction of γ-beam propagation, and $N_A = 6.02 \times 10^{23}$ represents Avogadro's constant.

In our simulation, for a certain geometry of an isotopic target, we sampled a certain γ-ray photon with energy $E_{\gamma,i}$ and position r_i recorded at the surface of the isotopic target, as discussed later. Accordingly, the cross section $\sigma(E_{\gamma,i})$ and the attenuation coefficient μ_i were obtained using a linear interpolation method. Given that the position r_i satisfies $r_i \leq R$ we calculated the reaction probability for the ith γ -photon interacting with the isotope inside the target as:

$$p_i = \frac{\rho N_A}{\mu_i M} \sigma(E_{\gamma,i})[1 - \exp(-\mu_i L)], \quad (3)$$

Otherwise, for $r_i > R$ the nuclear transmutation process does not occur and the resulting p_i equals to zero. Then we obtained the production rate of the product isotope to be:

$$P_0 = \frac{I}{N} \sum_{i=1}^{N} p_i. \quad (4)$$

Here, N is the total sampling number and I is the γ-beam flux at the surface of the isotopic target, the unit is photons/s.

The specific activity (A/m) is one of the most important quality criteria for radioisotopes production for nuclear medicine research and application. Here, A is the activity and m stands for the mass. When a γ-beam of high intensity triggers the isotopic target into the product of interest and considering that any other reactions (such as destruction of the product by nuclear reactions) do not interfere significantly, the specific activity for the product isotope is given by:

$$\left(\frac{A}{m}\right)_{\mathrm{product}} = \frac{P_0}{m}[1 - \exp(-\lambda_1 t_{\mathrm{irr}})], \quad (5)$$

where $\lambda_1 = \ln(2)/T_{1/2}$ is the decay constant of the product isotope with a half-life of $T_{1/2}$, and t_{irr} is the irradiation time. For some specific cases, the daughter of the product isotope rather than itself is of particular interest for medical applications. The product isotope is only used as a radionuclide generator. The most prominent example is the ^{99}Mo/^{99m}Tc generator, which is usually produced by a neutron-induced fission process, or by photoneutron reaction and its disintegration, $^{100}\mathrm{Mo}(\gamma, n)^{99}\mathrm{Mo} \rightarrow {}^{99m}\mathrm{Tc}$. For the latter, we derived the specific activity of the daughter radionuclide from the decay law:

$$\left(\frac{A}{m}\right)_{\mathrm{daughter}} = \frac{P_0}{m}\left[1 + \frac{\lambda_1 \exp(-\lambda_2 t_{\mathrm{irr}}) - \lambda_2 \exp(-\lambda_1 t_{\mathrm{irr}})}{\lambda_2 - \lambda_1}\right], \quad (6)$$

where λ_2 corresponds to the decay constant of the daughter radioisotope. If the generator radioisotope has a smaller decay constant than its daughter radioisotope, then a radioactive decay equilibrium between them could be achieved and hence one could optimize the irradiation time to achieve sufficient specific activities of the radioisotopes of interests.

3 Results

3.1 ^{99}Mo/^{99m}Tc radioisotopes production

Typically, molybdenum and its isotopes exist in the form of oxide on Earth. We considered a pure solid oxide $^{100}MoO_3$ as the irradiation target with a density of 4.7 g/cm^3. The ^{100}Mo isotope has an extremely long half-life, $T_{1/2} = 7.3 \times 10^{18}$ years and therefore is very stable. The isotope ^{99}Mo, the product of ^{100}Mo(γ, n) reaction, is a natural beta emitter, decaying spontaneously into ^{99m}Tc which further emits 140.5 keV γ-ray by internal conversion to the ground state. The production of ^{99m}Tc and the disintegration chain of ^{99}Mo is shown in Fig. 3.

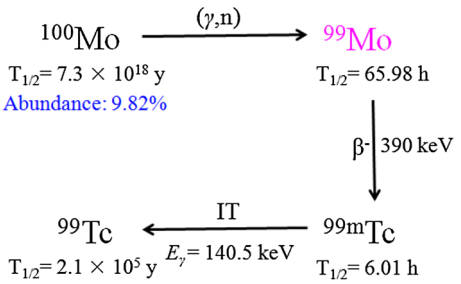

Fig. 3 ^{99m}Tc production via ^{100}Mo(γ, n) reaction and disintegration chain of ^{99}Mo

Existing measurements of (γ, γ') photo-absorption cross sections up to the neutron-separation energy and of partial (γ, n), $(\gamma, 2n)$ and $(\gamma, 3n)$ photoneutron cross sections for ^{100}Mo retrieved from the EXFOR database [26] are presented in Fig. 4 together with the corresponding EMPIRE calculations [30] and the existing TENDL evaluation [31]. Very good agreement can be observed between the EMPIRE calculations and the (γ, γ') and (γ, n) measurements [32–34] at energies up to two neutron emission threshold. The TENDL evaluation overestimates the measured cross sections below the energy of the (γ, n) cross section peak. Both the (γ, n) cross section peak value and its corresponding energy given by TENDL are lower than the experimental ones. The $(\gamma, 2n)$ cross sections are slightly overestimated by both the EMPIRE calculations and the TENDL evaluations. The EMPIRE calculations are in good agreement with the $(\gamma, 3n)$ measurements, while the TENDL evaluations overestimate them. Thus based on the good agreement between the EMPIRE calculations and the measured cross section for the (γ, n) reaction, which is the reaction of interest for the production of ^{99m}Tc, we decided to use the results of the EMPIRE code for our induced activity calculations, which provided a 150-mb peak of the ^{100}Mo(γ, n) reaction cross section at $E_\gamma = 14.5$ MeV.

Figure 5 shows the saturation specific activity of ^{99}Mo/^{99m}Tc radioisotopes as a function of the target geometry for different γ-beam energies as inputs. The 14.7 MeV γ-beam provided the highest specific activity compared with other γ-beam conditions. This was mainly caused by the fact that the CBS γ-beam spectrum covers the energy, 14.5 MeV, that leads to a peaked GDR cross section in ^{100}Mo(γ, n) reaction. The calculations showed that the highest specific activity of approximately 1.8 mCi/g can be achieved for a thin target (radius $\leq$2.0 mm and thickness 1.0 cm). It is also shown in Fig. 5a that the thinner the isotopic target, the higher the specific activity.

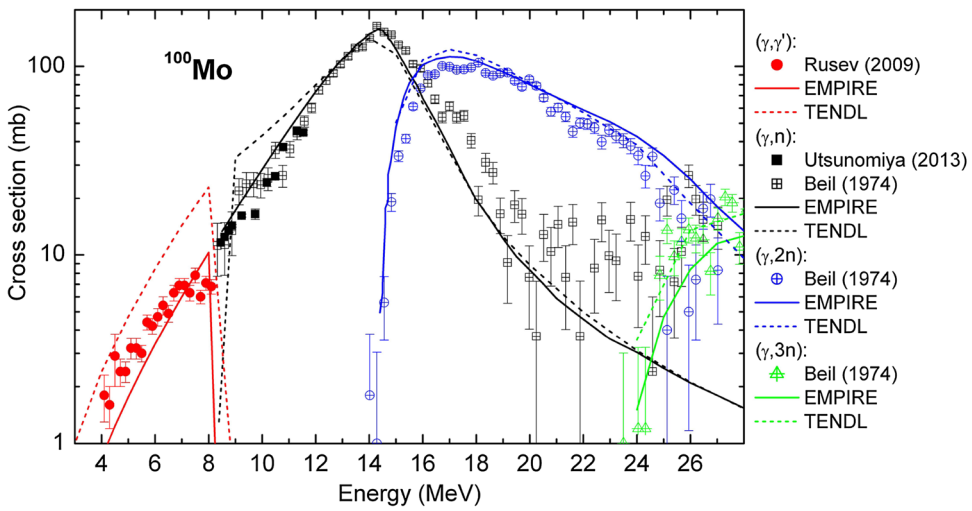

Fig. 4 Existing measurements of (γ, γ'), (γ, n), $(\gamma, 2n)$ and $(\gamma, 3n)$ cross sections for ^{100}Mo retrieved from the EXFOR database [26] together with corresponding EMPIRE calculations and the existing TENDL evaluation [31]. Experimental points in the figure are taken from Refs. [32–34], as indicated in the legend on the right-hand side of the figure

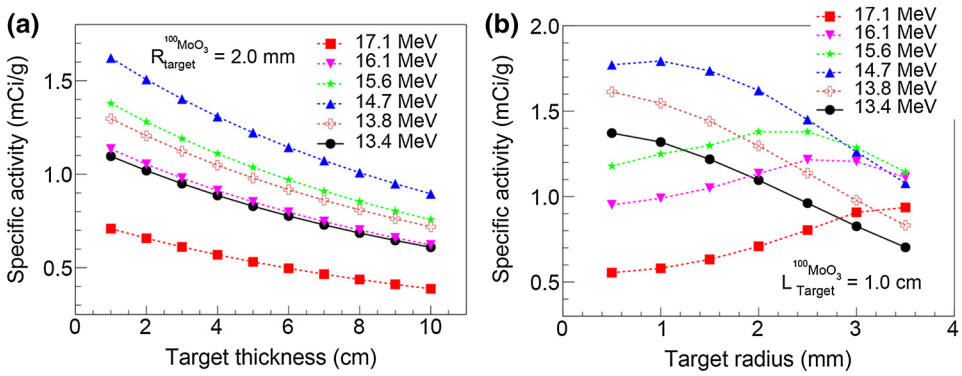

Fig. 5 Saturation specific activity of ^{99}Mo/^{99m}Tc radioisotopes as a function of the target thickness (**a**) and radius (**b**) for different γ-beam energies as inputs

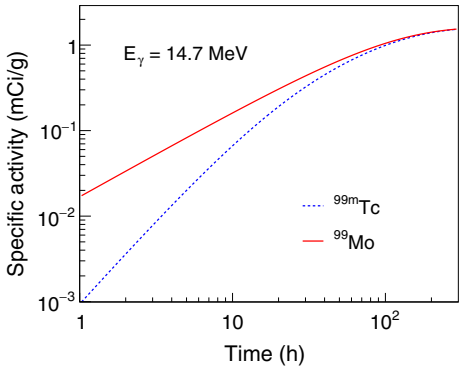

Fig. 6 Specific activity of ^{99}Mo/^{99m}Tc generator as a function of irradiation time. The input parameters for the isotopic target are 2.0 mm radius and 1.0 cm thickness

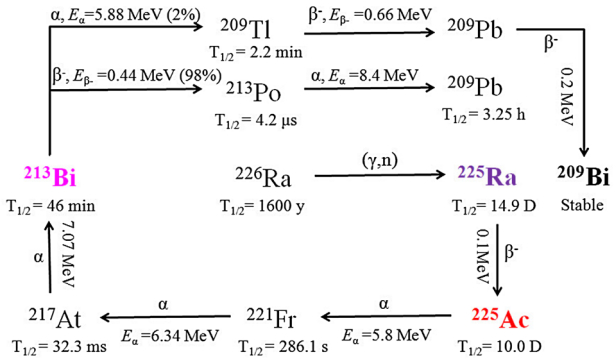

Fig. 7 Schematic of the ^{225}Ac radioisotope production and disintegration chain of ^{225}Ra via (γ, n) reaction

Figure 5b shows that for each γ-beam energy, the specific activity has an inflection point, where the highest specific activity was achieved. However, the position of such an inflection point is flexible and depends on the position of the intersection point in Fig. 2, due to the convolution between the γ-beam spectrum and the reaction cross section. Taking the ^{100}Mo(γ, n) reaction as an example, the inflection point occurred for a target radius of approximately 1.0 mm for the 14.7 MeV γ-beam, and 2.5 mm for the 16.1 MeV γ-beam, which is consistent with data shown in Fig. 2. Our simulations suggest that the matching the CBS γ-beam spectrum with a peaked photonuclear cross section by using an appropriate γ-beam may provide an effective approach to producing medical radioisotope with a maximum specific activity.

Figure 6 shows the specific activities of ^{99}Mo isotope and its daughter ^{99m}Tc as a function of the irradiation time. Using an optimal γ-beam energy (14.7 MeV) and a thin target (radius 1–2 mm, thickness 1 cm), the specific activities of the ^{99}Mo and ^{99m}Tc isotopes reached 0.36 and 0.24 mCi/g, respectively, after one day irradiation, while their saturation specific activities exceeded 1.6 mCi/g after more than 5–6 times half-life irradiation interval.

3.2 ^{225}Ra/^{225}Ac radioisotopes production

Among the α-emitters which can be produced at ELI–NP facility, a radioisotope of interest is ^{225}Ac ($T_{1/2} = 14.8$ days). It disintegrates to ^{209}Bi ($T_{1/2} = 1.9 \times 10^{19}$ years) by a series of four alpha and two β^- decays, as shown in Fig. 7. The radioisotope ^{225}Ac can be used directly for targeted alpha therapy or as a generator for ^{213}Bi, which in turn can also be used for the same purpose. Thus, we propose the following production route for ^{225}Ac: ^{226}Ra$(\gamma, n)^{225}$Ra $\rightarrow$ ^{225}Ac, since ^{225}Ra naturally decays to ^{225}Ac and can be separated chemically from the ^{226}Ra target (^{225}Ra/^{225}Ac generator). A metallic ^{226}Ra isotope target with a density of 5.0 g/cm^3 was used in the simulation.

Since no experimental data on γ-induced reactions on ^{226}Ra are currently available within the EXFOR database, the cross sections calculated using the EMPIRE are compared in Fig. 8 with the existing TENDL evaluation for the (γ, n), (γ, 2n) and for the total photo-absorption cross section. For the (γ, n) reaction, the TENDL evaluation provides a lower peak cross section, a larger curve width and a higher peak energy than the EMPIRE calculations. We decided to use the TENDL evaluation for our induced

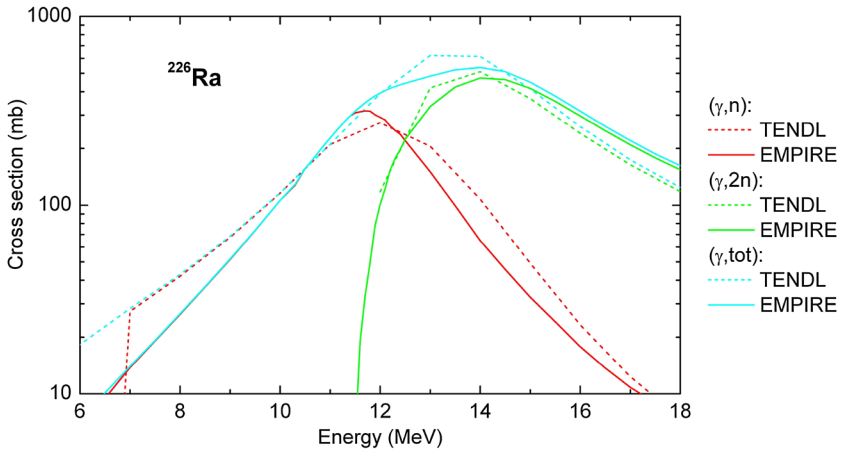

Fig. 8 EMPIRE calculations and the existing TENDL evaluation for the (γ, n), $(\gamma, 2n)$ and for the total photo-absorption cross section on ^{226}Ra

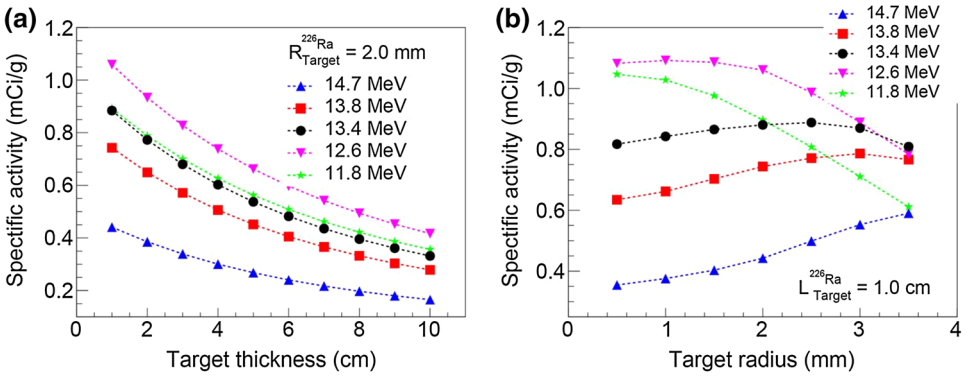

Fig. 9 Saturation specific activity of the ^{225}Ra/^{225}Ac radioisotopes as a function of the target thickness (**a**) and radius (**b**) for different γ-beam energies

activity calculations, which provides a relatively high peak cross section, ∼290 mb, for the ^{226}Ra(γ, n) reaction at $E_\gamma = 12$ MeV.

Figure 9 shows the saturation specific activity of the ^{225}Ra/^{225}Ac generator as a function of the isotopic target thickness and radius. The 12.6 MeV γ-ray beam is suitable for triggering the ^{226}Ra(γ, n) reaction, generating the highest specific activity of α-emitters, including ^{225}Ac and its daughter radioisotopes. Figure 9b also shows that for the 11.8 and 12.6 MeV γ-ray beams, the specific activity increased as the target radius decreased. For γ-beams with energy $E_\gamma \geq 13.4$ MeV, the inflection point of the specific activity occurred at a target radius ≥2.5 mm, which correlated closely with their maximum specific activities. It is also demonstrated in Fig. 9b that if the appropriate isotopic target and γ-beam parameters were employed, the saturation activity for ^{225}Ra/^{225}Ac generator exceeded 1.1 mCi/g.

3.3 ^{186}Re radioisotopes production

The possibility for the production of the ^{186}Re radioisotope with intense γ-ray beams was also investigated by using the ^{187}Re(γ, n) reaction. While ^{187}Re is a stable isotope with a high natural abundance of 62.6 %, ^{186}Re is a radioisotope that emits electrons with the average energy of about

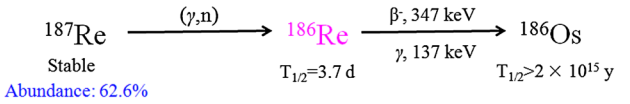

Fig. 10 Schematic of the ^{186}Re radioisotope production via (γ, n) reaction

350 keV and a 137 keV γ-ray line, as shown in Fig. 10. Existing data for cross sections for the ^{187}Re(γ, n) reaction and for the (γ, Sn) photoneutron yield reaction defined as:

$$\sigma(\gamma, Sn) = \sigma(\gamma, n) + \sigma(\gamma, np) + 2 \cdot \sigma(\gamma, 2n), \quad (7)$$

are presented in Fig. 11 together with the corresponding EMPIRE calculation and the existing TENDL evaluation. The recent (γ,n) reaction cross section measurement performed using quasi-monochromatic γ-ray beams at the TERAS electron storage ring [35] yielded lower values than that obtained using continuous bremsstrahlung γ-ray beams [36] and was in better agreement with the EMPIRE calculation. The bremsstrahlung data are well reproduced by the TENDL evaluation for energies below (γ, n) peak energy. Above the peak energy, the bremsstrahlung data are in good agreement with the EMPIRE calculation and are overestimated by the TENDL evaluation.

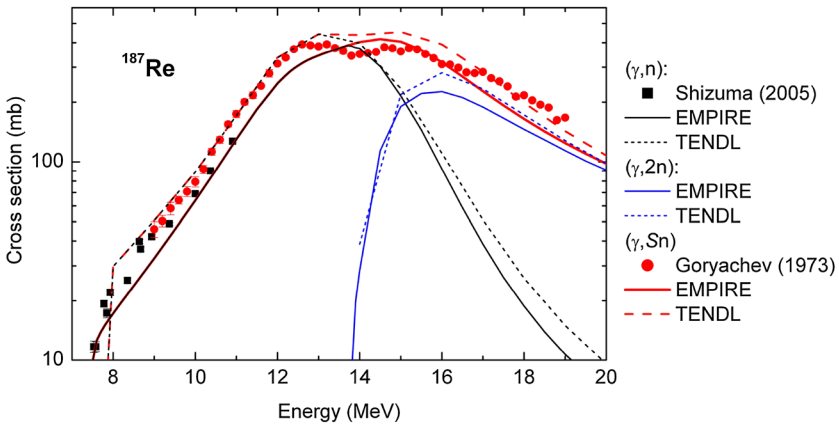

Fig. 11 Existing measurements for the (γ, Sn) photoneutron yield reaction cross section, as defined by Eq. (7), and for the (γ, n) reaction cross section on ^{187}Re together with corresponding EMPIRE calculations and the existing TENDL evaluation. Experimental points in the figure are taken from Refs. [35, 36], as indicated in the legend on the right-hand side of the figure

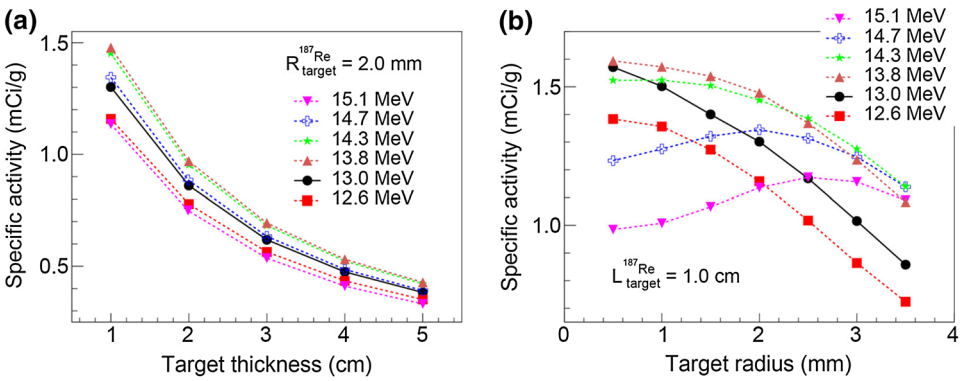

Fig. 12 Saturation specific activity of the ^{186}Re radioisotope as a function of the target thickness (**a**) and radius (**b**) for different γ-beam energies

We have decided to use the TENDL evaluation for our study, since there was an overall good agreement with the bremsstrahlung photoneutron data. The calculations provided a 430-mb peak cross section at $E_\gamma = 13$ MeV. It is interesting to note that the energy at the peak cross section is exactly covered by the γ-ray energy region at the ELI–NP facility and will be possible to be measured in detail. In the simulations, we considered that the metallic ^{187}Re target has a density of 21.04 g/cm^3.

The saturation specific activity of ^{186}Re radioisotope as a function of the target thickness and radius is shown in Fig. 12. Choosing an isotopic target with a radius smaller than 2.5 mm, the 13.8 MeV γ-beam, which involved the best convolution between the γ-beam spectrum and the induced reaction cross section, resulted in the highest specific activity. The saturation specific activity for ^{186}Re radioisotope exceeded 1.5 mCi/g when using optimal irradiation conditions, e.g., a 13.8 MeV γ-beam and a target with a radius ∼2.0 mm and a thickness of 1.0 cm.

4 Discussion

In this paper, we modeled through Monte Carlo simulations the ELI–NP γ-beam interaction with a solid target and we estimated the radioisotope production parameters for ^{99}Mo/^{99m}Tc,^{225} Ra/^{225}Ac and ^{186}Re which are not available in the literature. We presented in detail the results (Sect. 3) of such simulation using the calculated CBS γ-beam parameters. We have optimized the isotopic target dimensions and the beam parameters, at defined irradiation time intervals, to maximize the isotope production. This study is especially important because a number of radioisotopes of medical interest were previously produced by nuclear reactors and alternative production routes are currently evaluated. In addition, the application of ^{225}Ra/^{225}Ac,^{186} Re and other isotopes in targeted therapy is promising and the investigation of the new production route by (γ, n) reaction at ELI–NP is feasible.

^{225}Ac is an alpha emitter important for targeted alpha therapy. Currently the ^{225}Ac is produced by decay of ^{225}Ra (^{235}U chain) or by reaction ^{226}Ra(n, 2n)^{225}Ra → ^{225}Ac and is available in very small amounts (about 1 Ci per year), which is very little compared to the need for large scale application. Its daughter ^{213}Bi can be also used for targeted alpha therapy with a high energy of 8.4 MeV. These radioisotopes are usually used in combination with peptides with short uptake time and with antibodies seeking blood cancer cells. With a monoclonal antibody that interferes with the HER2/neu receptor, it has proved

Table 1 A brief summary of the potential radioisotopes of medical interest that can be produced by ELI–NP γ-beam

Product isotope	$T_{1/2}$ (day)	(γ,n) target	m[a] (g)	σ_{peak} (Barn)	$E_{\gamma,peak}$[b] (MeV)	Cross section width (MeV)	E_γ (MeV)	γ-Beam flux (s^{-1})	A/m[c] (mCi/g)	Amount per day (MBq)
^{99m}Tc	0.25	$^{100}MoO_3$	0.40	0.15	14.5	2.09	14.7	10^{11}	1.6	8.9
^{186}Re	3.7	^{187}Re	2.64	0.43	13.0	1.72	13.8	10^{11}	1.5	24.7
^{225}Ac	10.0	^{226}Ra	0.63	0.29	12.0	1.65	12.6	10^{11}	1.1	1.2

[a] An isotopic target with 2.0 mm radius and 1.0 cm thickness was used for calculation

[b] Corresponds to the γ-ray energy at the peak of the reaction cross section

[c] Corresponds to the saturation specific activity after a long enough irradiation integral

effective in: leukemia, lymphoma, breast, ovarian, neuroblastoma and prostate cancers [37]. The other radioisotope investigated, ^{186}Re, is used with a high specific activity for antibody and peptide radiolabelling [38], preparation of phosphonates for bone pain palliation [39] and its use for intravascular radiotherapy for inhibition of coronary restenosis after angioplasty is also possible with a lower specific activity.

In order to summarize our results, we present in Table 1 the optimum values of the on-axis γ-beam energy (E_γ) at a CBS γ-beam facility, with respect to the energy ($E_{\gamma,peak}$) at the peak of the reaction cross section (σ_{peak}) for the above discussed radioisotopes. Table 1 also shows the estimates of the achievable specific activities for ^{99}Mo/^{99m}Tc,^{225} Ra/^{225}Ac and ^{186}Re radioisotopes which are of the order of a few mCi/g for thin targets with about one gram of mass, a γ-beam flux of 10^{11}s^{-1} and a beam radius of 2.5 mm for an optimized γ-beam energy.

Apart from target geometry, γ-beam flux and optimization of the γ-beam energy, the convolution between the γ-beam spectrum and the reaction cross section plays also an important role in the determination of the maximum specific activity. Using the optimized γ-beam energy and target geometry from Table 1, the saturation specific activity of the ^{99}Mo/^{99m}Tc,^{186} Re and ^{225}Ra/^{225}Ac radioisotopes as a function of the bandwidth ratio is shown in Fig. 13. Here, the bandwidth ratio was defined as the ratio of the γ-beam bandwidth with respect to the reaction cross section width from Table 1. We calculated that as the maximum specific activity decreased with 30 %, the γ-beam r.m.s bandwidth values of 4.5 % for ^{99}Mo/^{99m}Tc and 5.1 % for ^{186}Re and ^{225}Ra/^{225}Ac were required. Accordingly, the bandwidth ratio was calculated to be about 0.3–0.4 (Fig. 13). This ratio may be useful for the evaluation of other radioisotope production cases.

We discuss here also the optimal target thickness L correlated with the target density, ρ, and the implications for the specific activity of the radioisotope. The γ-beam is attenuated while interacting with the target and the value of the mass attenuation coefficient (μ_m) is approximately

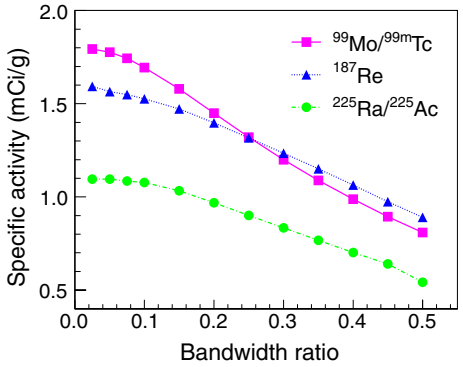

Fig. 13 Saturation specific activity of the ^{99}Mo/^{99m}Tc,^{186} Re and ^{225}Ra/^{225}Ac radioisotopes as a function of the bandwidth ratio. The input γ-beam energy is 14.7, 13.8 and 12.6 MeV, respectively

constant for a given quasi-monochromatic γ-beam and a specified target. Then, based on the results from Figs. 5a, 9a and 12a at 70 % of the maximum specific activity the target thickness should satisfy:

$$L = f/\mu_m \rho, \tag{8}$$

where the factor f ranges from 0.8 to 0.9 depending on the specific radioisotope.

Concerning the energy that is transferred to the target and its subsequent heating by the γ-beam, it may or not be significant, such to lead to melting of the target and this could be evaluated through additional calculations. However, for the specific cases considered in the study, ^{100}Mo oxide and ^{226}Ra have the melting points at 795 and 699.8 °C respectively, while ^{187}Re melts at 3182 °C. Taking into account the relative low melting points for the first two targets, a multiple thin target setup which allows the electrons and positrons, produced by Compton scattering and by pair creation, to leave the targets rapidly, and a water cooling blanket could be used to decrease the heating and to avoid the melting.

In this study, a γ-beam flux of 10^{11} s^{-1} was used. However, the ELI–NP facility will deliver a γ-beam flux of about 10^{12} s^{-1} and thus a saturation specific activity of

tens mCi/g could be obtained. With further increase in the γ-beam flux, from 10^{11} s^{-1} to more than 10^{14} s^{-1}, it would be possible to produce sufficient amounts of the radioisotopes discussed (several GBq per day), and secondly it will provide unprecedented opportunities for medical and biomedical research with innovative isotopes like ^{47}Sc,^{67} Cu and ^{225}Ac [4].

5 Conclusion and outlook

We have shown in this paper that the production through photonuclear reactions of ^{99}Mo/^{99m}Tc,^{225} Ra/^{225}Ac and ^{186}Re radioisotopes (taken as examples) is possible for optimized γ-beam energy, target geometry and γ-beam bandwidth. We estimated through Monte Carlo simulations that a specific activity of the order of 1–2 mCi/g can be achieved for a thin target (radius 1–2 mm, thickness 1 cm, and around one gram of mass) and a γ-beam flux of 10^{11} s^{-1}. The convolution between the γ-beam spectrum and the reaction cross section, and an optimal target thickness for specific activity of the radioisotopes, were also demonstrated. We conclude that the ELI–NP facility will provide an unprecedented possibility for the production of new radioisotopes in sufficient quantities for nuclear medicine research.

The ELI–NP cannot be, based on current estimations, a radioisotope production facility. Such a production facility would need to provide thousands of patient doses per day and thus much higher specific activities of 0.1 TBq. However, future γ-beams facilities may have the capabilities to obtain radioisotopes with required higher activities for clinical use. Concerning to reduce their radioisotope production cost, one possibility would be to use the facility in parallel, not only for production with multiple targets placed along the direction of the collimated, high-intensity γ-beam, but also for nuclear physics research. Another fact that should be considered is that the main production route for radioisotopes was by nuclear reactors that had increased costs for dealing with large amounts of nuclear waste. A γ-beam facility would generate almost no nuclear waste and thus will have very low costs for solving this problem. Benefiting from the high-quality, high-intensity γ-beam provided by the ELI–NP, the photonuclear reaction can be viewed as a new production scheme for radioisotopes of medical interest, which may be competitive to classical production schemes such as nuclear fission and charged-particle reactions with *p*, *d* or alpha ions.

While other facilities do have enough capabilities to decrease the gap between demand and supply for ^{99}Mo/^{99m}Tc, this benchmark case will be considered only for testing the prototype facility concerning the new methods of radioisotope production at ELI–NP, since its separation processes and the associated technology are well established. Further, the production of isomers such as ^{195m}Pt,^{115m} In,^{176m} Lu and ^{87m}Sr is also of great interest. Due to a low gateway state for some key nuclides [40], it would be possible to explore the direct activation of the above-mentioned nuclides using the low-energy γ-beam, below 3.5 MeV, at ELI–NP.

Finally, various irradiation experiments of thin targets with a γ-beam, in which the specific activity of product radioisotopes will be determined, could be used to perform reaction cross section measurements. Since the ELI–NP facility could provide a much higher γ-beam flux than that produced by other available γ-beam facilities, it will be possible to make precise cross section experimental measurements for many isotopes [35], especially for those isotopes with unknown or low cross sections.

Acknowledgments This work is supported by Extreme Light Infrastructure – Nuclear Physics (ELI–NP)-Phase I, a project co-financed by the European Union through the European Regional Development Fund. WL thanks the supports from the National Natural Science Foundation of China (Grant No. 11405083) and the Young Talent Project of the University of South China.

References

1. World Nuclear Association, *Radioisotopes in Medicine* (Information Library, 2014)
2. C. Schiepers, *Diagnostic Nuclear Medicine* (Springer, Berlin, 2006)
3. NuPECC Report, *Nuclear Physics for Medicine*. http://www.nupecc.org/pub/npmed2014
4. D. Habs, U. Köster, Appl. Phys. B **103**, 501–519 (2011)
5. G.A. Mourou, C.L. Labaune, M. Dunne, N. Naumova, V.T. Tikhonchuk, Plasma Phys. Control. Fusion **49**, B667 (2007)
6. W.K.W.D. Ledingham, P. McKenna, R.P. Singhal, Science **300**, 1107 (2003)
7. K. Ta Phuoc, S. Corde, C. Thaury, V. Malka, A. Tafzi, J.P. Goddet, R.C. Shah, S. Sebban, A. Rousse, Nat. Photonics **6**, 308 (2012)
8. W.J. Brown, S.G. Anderson, C.P.J. Barty, S.M. Betts, R. Booth, J.K. Crane, D.N. Fiffinghoff, D.J. Gibson, F.V. Hartmann, E.P. Hartouni, J. Kuba, G.P. Le Sage, D.R. Slaughter, A.M. Tremaine, A.J. Wootton, P.T. Springer, Phys. Rev. ST AB **7**, 060702 (2004)
9. K. Chouffani, D. Wells, F. Harmon, J. Jones, G. Lancaster, Nucl. Instrum. Methods Phys. Res. A **495**, 95 (2002)
10. M. Babzien, I. Ben-Zvi, K. Kusche, I.V. Pavlishin, I.V. Pogorelsky, D.P. Siddons, V. Yakimenko, D. Cline, F. Zhou, T. Hirose, Y. Kamiya, T. Kumita, T. Omori, J. Urakawa, K. Yokoya, Phys. Rev. Lett. **96**, 054802 (2006)
11. W. Luo, W. Xu, Q.Y. Pan, X.Z. Cai, J.G. Chen, Y.Z. Chen, G.T. Fan, G.W. Fan, W. Guo, Y.J. Li, W.H. Liu, G.Q. Lin, Y.G. Ma, W.Q. Shen, X.C. Shi, B.J. Xu, J.Q. Xu, Y. Xu, H.O. Zhang, Z. Yan, L.F. Yang, M.H. Zhao, Rev. Sci. Instrum. **81**, 013304 (2010)
12. W. Luo, W. Xu, Q.Y. Pan, X.Z. Cai, Y.Z. Chen, G.T. Fan, G.W. Fan, Y.J. Li, W.H. Liu, G.Q. Lin, Y.G. Ma, W.Q. Shen, X.C. Shi, B.J. Xu, J.Q. Xu, Y. Xu, H.O. Zhang, Z. Yan, L.F. Yang, M.H. Zhao, Appl. Phys. B **101**, 761 (2010)
13. S. Chen, N.D. Powers, I. Ghebregziabher, C.M. Maharjan, C. Liu, G. Golovin, S. Banerjee, J. Zhang, N. Cunningham, A.

Moorti, S. Clarke, S. Pozzi, D.P. Umstadter, Phys. Rev. Lett. **110**, 155003 (2013)
14. G. Sarri, D.J. Corvan, W. Schumaker, J.M. Cole, A. Di Piazza, H. Ahmed, C. Harvey, C.H. Keitel, K. Krushelnick, S.P.D. Mangles, Z. Najmudin, D. Symes, A.G.R. Thomas, M. Yeung, Z. Zhao, M. Zepf, Phys. Rev. Lett. **113**, 224801 (2014)
15. W. Luo, W. Xu, Q.Y. Pan, Z.D. An, X.L. Cai, G.T. Fan, G.W. Fan, Y.J. Li, B.J. Xu, Z. Yan, L.F. Yang, Nucl. Instrum. Methods Phys. Res. A **660**, 108–115 (2011)
16. http://www.tunl.duke.edu/higs/
17. J.L. Tain, Synchrotron Radiat. News **22**, 3 (2009) **(and reference therein)**
18. Q.Y. Pan, W. Xu, W. Luo, X.Z. Cai, J.G. Chen, G.T. Fan, G.W. Fan, W. Guo, Y.J. Li, G.Q. Lin, Y.G. Ma, W.Q. Shen, X.C. Shi, H.W. Wang, B.J. Xu, J.Q. Xu, Y. Xu, Z. Yan, L.F. Yang, M.H. Zhao, Synchrotron Radiat. News **22**, 11 (2009) **(and reference therein)**
19. Y. Glinec, J. Faure, L. Le Dain, S. Darbon, T. Hosokai, J.J. Santos, E. Lefebvre, J.P. Rousseau, F. Burgy, B. Mercier, V. Malka, Phys. Rev. Lett. **94**, 025003 (2005)
20. P.A. Norreys, M. Santala, E. Clark, M. Zepf, I. Watts, F.N. Beg, K. Krushelnick, M. Tatarakis, A.E. Dangor, X. Fang, P. Graham, T. McCanny, R.P. Singhal, K.W.D. Ledingham, A. Creswell, D.C.W. Sanderson, J. Magill, A. Machacek, J.S. Wark, R. Allott, B. Kennedy, D. Neely, Phys. Plasmas **6**, 2150 (1999)
21. A. Giulietti, N. Bourgeois, T. Ceccotti, X. Davoine, S. Dobosz, P. D'Oliveira, M. Galimberti, J. Galy, A. Gamucci, D. Giulietti, L.A. Gizzi, D.J. Hamilton, E. Lefebvre, L. Labate, J.R. Marques, P. Monot, H. Popescu, F. Reau, G. Sarri, P. Tomassini, P. Martin, Phys. Rev. Lett. **101**, 105002 (2008)
22. W. Schumaker, G. Sarri, M. Vargas, Z. Zhao, K. Behm, V. Chvykov, B. Dromey, B. Hou, A. Maksimchuk, J. Nees, V. Yanovsky, M. Zepf, A.G.R. Thomas, K. Krushelnick, Phys. Plasmas **21**, 056704 (2014)
23. D. Habs, T. Tajima, J. Schreiber, C. Barty, M. Fujiwara, P. Thirolf, Eur. Phys. J. D **55**, 279 (2009)
24. D. Habs, P.G. Thirolf, C. Lang, M. Jentschel, U. Köster, F. Negoita, V. Zamfir, Proc. SPIE **8079**, 80791H (2011)
25. http://www.eli-np.ro/ (2015)
26. IAEA Nuclear data services. https://www-nds.iaea.org/exfor/exfor.htm and https://www-nds.iaea.org/exfor/endf.htm
27. I. Gheorghe et al., Laser Compton scattering simulation code **(to be published)**
28. S. Agostinelli, and Geant4 Collaboration. Nucl. Instr. Methods A **506**, 250 (2003)
29. M. Herman, R. Capote, B.V. Carlson, P. Oblozinsky, M. Sin, A. Trkov, H. Wienke, V. Zerkin, EMPIRE: nuclear reaction model code system for data evaluation. Nuclear Data Sheets **108**, 2655 (2007). www-nds.iaea.org/empire/index.html
30. R. Capote, M. Herman, P. Oblozinsky, P.G. Young, S. Goriely, T. Belgya, A.V. Ignatyuk, A.J. Koning, S. Hilaire, V.A. Plujko, M. Avrigeanu, O. Bersillon, M.B. Chadwick, T. Fukahori, Ge Zhigang, S. Yinlu Han, J. Kailas, V.M. Kopecky, G. Maslov, M. Reffo, E. Sin, Sh Soukhovitskii, P. Talou, Nucl. Data Sheets **110**, 3107 (2009)
31. A.J. Koning, D. Rochman. ftp://ftp.nrg.eu/pub/www/talys/tendl2010/tendl2010.html
32. G. Rusev, R. Schwengner, R. Beyer, M. Erhard, E. Grosse, A.R. Junghans, K. Kosev, C. Nair, K.D. Schilling, A. Wagner, F. Dönau, S. Frauendorf, Phys. Rev. C **79**, 061302 (2009)
33. H. Utsunomiya, S. Goriely, T. Kondo, C. Iwamoto, H. Akimune, T. Yamagata, H. Toyokawa, H. Harada, F. Kitatani, Y.-W. Lui, A.C. Larsen, M. Guttormsen, P.E. Koehler, S. Hilaire, S. Pru, M. Martini, A.J. Koning, Phys. Rev. C **88**, 015805 (2013)
34. H. Beil, R. Bergère, P. Carlos, A. Leprêtre, A. De Miniac, A. Veyssière, Nucl. Phys. A **227**, 427–449 (1974)
35. T. Shizuma, H. Utsunomiya, P. Mohr, T. Hayakawa, S. Goko, A. Makinaga, H. Akimune, T. Yamagata, M. Ohta, H. Ohgaki, Y.-W. Lui, H. Toyokawa, A. Uritani, S. Goriely, Phys. Rev. C **72**, 025808 (2005)
36. A.M. Goryachev, G.N. Zalesny, S.F. Smeenko, B.A. Tulupov, Yadernaya Fizika **17**, 463 (1973)
37. A.M. Ballangrud, W.-H. Yang, St Palm, R. Enmon, P.E. Borchardt, V.A. Pellegrini, M.R. McDevitt, D.A. Scheinberg, G. Sgouros, Clin. Cancer Res. **10**, 4489 (2004)
38. F.B. van Gog, G.W.M. Visser, R. Klok, R. van der Schors, G.B. Snow, G.A.M.S. van Dongen, J. Nucl. Med. **37**, 352–362 (1996)
39. Jac M.S.P. Quirijnen, Shiuw H. Han, Bernard A. Zonnenberg, John M.H. de Kierk, Alfred D. van het Schip, Aalt van Dijk, Herman F.J. ten Kroode, Geert H. Blijham, Peter P. van Rijk, J. Nucl. Med. **37**, 1511–1515 (1996)
40. J.J. Carroll, M.J. Byrd, D.G. Richmond, T.W. Sinor, K.N. Taylor, W.L. Hodge, Y. Paiss, C.D. Eberhard, J.A. Anderson, C.B. Collins, Phys. Rev. C **43**, 1238 (1991)